

Electrically tuning exciton polaritons in a liquid crystal microcavity based on WS_2 monolayer

Chenxi Yang(杨晨曦), Lanyu Huang(黄岚雨), Yujie Li(李宇杰), Xiaokun Zhai(翟晓坤), Qiang Ai(艾强), Chunzi Xing(邢淳梓), Xinmiao Yang(杨新苗), Yazhou Gu(谷亚舟), Peigang Li(李培刚), Zhitong Li(李志瞳), Haitao Dai(戴海涛), Liefeng Feng(冯列峰), Linsheng Liu(刘林生), Xiao Wang(王笑), and Tingge Gao(高廷阁)
Citatio: Chin. Phys. B, 2025, 34 (**9**): 097803. DOI: 10.1088/1674-1056/ade668
http://cpb.iphy.ac.cn; http://iopscience.iop.org/cpb

What follows is a list of articles you may be interested in

Effects of helium ion irradiation and thermal annealing on the optical and structural properties of hexagonal boron nitride

Guan-Lin Liu(刘冠麟), Ji-Lian Xu(徐辑廉), Peng-Tao Jing(景鹏涛), Jing-Jing Shao(邵京京), Xu Guo(郭旭), Yun-Tao Wu(吴韵涛), Feng Qin(覃凤), Zhen Cheng(程祯), Deming Liu(刘德明), Yang Bao(鲍洋), Hai Xu(徐海), Li-Gong Zhang(张立功), Da Zhan(詹达), Jia-Xu Yan(闫家旭), Lei Liu(刘雷), and De-Zhen Shen(申德振)
Chin. Phys. B, 2025, 34 (**5**): 057801. DOI: 10.1088/1674-1056/adbee7

Unveiling localized electronic properties of ReS_2 thin layers at nanoscale using Kelvin force probe microscopy combined with tip-enhanced Raman spectroscopy

Yu Luo(罗宇), Weitao Su(苏伟涛), Juanjuan Zhang(张娟娟), Fei Chen(陈飞), Ke Wu(武可), Yijie Zeng(曾宜杰), and Hongwei Lu(卢红伟)
Chin. Phys. B, 2023, 32 (**11**): 117801. DOI: 10.1088/1674-1056/ace425

Multifunctional light-field modulation based on hybrid nonlinear metasurfaces

Shuhang Qian(钱树航), Kai Wang(王凯), Jiaxing Yang(杨加兴), Chao Guan(关超), Hua Long(龙华), and Peixiang Lu(陆培祥)
Chin. Phys. B, 2023, 32 (**10**): 107803. DOI: 10.1088/1674-1056/acdc13

Enhanced photoluminescence of monolayer MoS_2 on stepped gold structure

Yu-Chun Liu(刘玉春), Xin Tan(谭欣), Tian-Ci Shen(沈天赐), and Fu-Xing Gu(谷付星)
Chin. Phys. B, 2022, 31 (**8**): 087803. DOI: 10.1088/1674-1056/ac657b

Multifunctional disk device for optical switch and temperature sensor

Bian Zhen-Yu (卞振宇), Liang Rui-Sheng (梁瑞生), Zhang Yu-Jing (张郁靖), Yi Li-Xuan (易丽璇), Lai Gen (赖根), Zhao Rui-Tong (赵瑞通)
Chin. Phys. B, 2015, 24 (**10**): 107801. DOI: 10.1088/1674-1056/24/10/107801

SPECIAL TOPIC — Exciton physics: Fundamentals, materials and devices

Electrically tuning exciton polaritons in a liquid crystal microcavity based on WS_2 monolayer

Chenxi Yang(杨晨曦)[1], Lanyu Huang(黄岚雨)[2], Yujie Li(李宇杰)[1], Xiaokun Zhai(翟晓坤)[1,†], Qiang Ai(艾强)[1], Chunzi Xing(邢淳梓)[1], Xinmiao Yang(杨新苗)[1], Yazhou Gu(谷亚舟)[3], Peigang Li(李培刚)[4], Zhitong Li(李志曈)[3], Haitao Dai(戴海涛)[1], Liefeng Feng(冯列峰)[1], Linsheng Liu(刘林生)[5], Xiao Wang(王笑)[2], and Tingge Gao(高廷阁)[1,‡]

[1] *Department of Physics, School of Science, Tianjin University, Tianjin* 300072, *China*

[2] *College of Materials Science and Engineering, Hunan University, Changsha* 410082, *China*

[3] *State Key Laboratory of Information Photonics and Optical Communications, School of Science, Beijing University of Posts and Telecommunications, Beijing* 100876, *China*

[4] *School of Integrated Circuits & State Key Laboratory of Information Photonics and Optical Communications, Beijing University of Posts and Telecommunications, Beijing* 100876, *China*

[5] *School of Electronic and Information Engineering/School of Integrated Circuits, Guangxi Normal University, Guilin* 541004, *China*

(Received 29 April 2025; revised manuscript received 8 June 2025; accepted manuscript online 20 June 2025)

Two-dimensional (2D) transition-metal dichalcogenide (TMD) monolayers based on become a promising platform to study photonics and optoelectronics. Electrically controlling the excitonic properties of TMD monolayers can be realized in different devices. In this work, we realize the strong coupling between the excitons of WS_2 monolayers and a photonic cavity mode in a liquid crystal microcavity. The formed exciton polaritons can be electrically tuned by applying voltage to the microcavity. Our work offers a way to study exciton–polariton manipulation based on TMD monolayers by electrical methods at room temperature.

Keywords: transition-metal dichalcogenide (TMD), microcavity, liquid crystal, exciton polariton

PACS: 78.67.–n, 78.55.–m, 71.36.+c, 42.70.Df

DOI: 10.1088/1674-1056/ade668 **CSTR:** 32038.14.CPB.ade668

1. Introduction

Two-dimensional (2D) transition-metal dichalcogenides (TMDs), such as WS_2, MoS_2, and WSe_2, have attracted extensive attention in recent years due to their unique electronic and optical properties.[1–3] Unlike their bulk counterparts, which typically exhibit indirect bandgaps, TMD monolayers possess direct bandgaps at the K and K' points of the Brillouin zone, leading to strong light–matter interactions.[4–6] These characteristics make them ideal candidates for next-generation optoelectronic and quantum photonic applications.[7] One of the most notable features of TMDs is their strong excitonic effect, with binding energies reaching hundreds of meV,[8] an order of magnitude higher than traditional group III–V semiconductors.[9] These excitons can strongly couple with cavity-confined photons to form exciton–polaritons,[10,11] hybrid light–matter quasiparticles with tunable dispersion and ultrafast dynamics.[12] In particular, WS_2 monolayers have been widely used due to their high quantum yield, sharp exciton resonances, and excellent chemical stability.[13]

Recent studies have demonstrated polariton condensation and ultralow-threshold lasing in WS_2 monolayers embedded in microcavities[14] constructed by distributed Bragg reflectors (DBR). These macroscopic quantum states realized at room temperature mark a significant step toward polariton circuits and low-power coherent light sources. However, most current efforts still rely on passive cavity designs, which limit the tunability of polariton energy dispersion and valley polarization properties. At the same time, researchers have made progress in electrically and optically tuning the excitonic properties of monolayers. For example, under circularly polarized excitation, spin-valley degeneracy breaking has been achieved in MoS_2 monolayers through exciton–exciton Coulomb interactions, enabling dynamic valley control without the need for high magnetic fields or intense laser pulses.[15] In addition, chemical passivation strategies, such as oleic acid (OA) treatment, have been shown to suppress nonradiative recombination and enhance both neutral and interlayer exciton photoluminescence (PL) in WS_2 and MoS_2, providing a promising path toward robust excitonic systems.[16,17]

Despite these advancements, achieving electrical control over exciton–polariton states in 2D-material-based microcavities remains a key challenge. Liquid crystal (LC) materials, owing to their dielectric anisotropy and tunability under electric fields, have been proven to be promising tunable media for

†Corresponding author. E-mail: xiaokunzhai@tju.edu.cn

‡Corresponding author. E-mail: tinggegao@tju.edu.cn

© 2025 Chinese Physical Society and IOP Publishing Ltd. All rights, including for text and data mining, AI training, and similar technologies, are reserved.

optical cavities.[18] Integrating LC layers into WS_2-based microcavity structures provides a viable approach to achieve *in situ* electrical control of exciton–polaritons, potentially combining the strong excitonic responses of TMDs with the tunability of LCs.

In terms of material synthesis, WS_2 monolayers are typically grown using chemical vapor deposition (CVD), a widely applied bottom-up synthesis technique for 2D materials. CVD offers strong controllability, large-area growth, high crystallinity, and precise thickness control.[19] During the CVD process, metallic precursors (tungsten oxide) and chalcogen sources (sulfur powder) are thermally evaporated in a carrier gas atmosphere and react on an insulating substrate to form TMD monolayers. Although CVD-grown monolayers often contain intrinsic defects that can reduce PL quantum efficiency and exciton coherence, the method remains capable of producing high-quality, large-area monolayers.[20]

In this work, we synthesized WS_2 monolayers using the CVD method and characterized their quality through PL and Raman spectroscopy. We then integrated the WS_2 monolayer with DBR to construct a Fabry–Pérot microcavity and introduced a liquid crystal as a tuning medium. This structure enables an electrically tunable exciton–polariton system based on monolayer WS_2. By applying an external electric field to an LC microcavity, we have successfully achieved electrical control of exciton–polaritons. Our system allows active control of strong coupling regimes and polarization-dependent optical responses, paving the way for reconfigurable polaritonic devices operable at room temperature.

2. Experimental details

We synthesized the WS_2 monolayers using the CVD method, as illustrated in Fig. 1(a). In this process, WO_3 powder (10 mg) was used as the metal oxide precursor and sulfur powder (200 mg) as the chalcogen source. The sulfur powder was placed upstream and the WO_3 powder downstream in the furnace. High-purity argon (99.999%) served as the carrier gas, with a constant flow rate of 100 sccm under atmospheric pressure. The temperature was ramped up to 1110 K at a rate of 20 °C/min and maintained for 10 minutes to facilitate the growth of WS_2 monolayers on SiO_2/Si substrates. These substrates were placed face-down above the WO_3 precursor to enhance monolayer uniformity and coverage.[21]

After obtaining suitable WS_2 monolayers, we employed a tape-assisted transfer method to prepare them for integration into a Fabry–Pérot microcavity, as shown in Fig. 1(b). First, we observed the WS_2 monolayers grown on SiO_2/Si substrates under an optical microscope and selected an appropriate region, recording its position. Then we pressed a piece of thermal release tape (TRT) onto the selected region with tweezers until it bonded firmly with the substrate. Next, we peeled off the tape, transferring the WS_2 monolayers onto the TRT. Using a home-made transfer platform, we aligned and transferred the monolayers onto a DBR, which we paired with another DBR to construct the optical microcavity. To minimize adhesion and contamination, the TRT/WS_2 stack was gently heated to 120 °C before release.

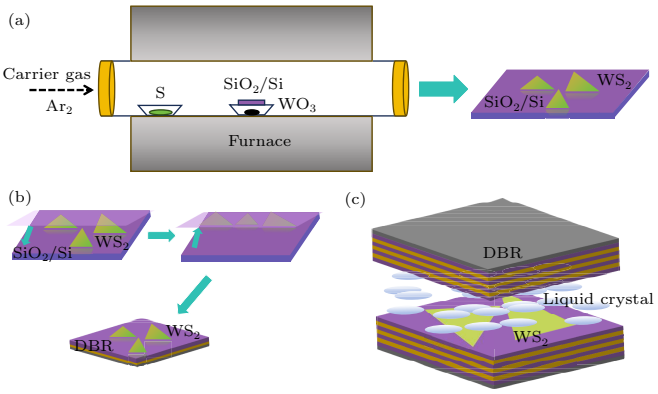


Fig. 1. Schematic of WS_2 monolayer synthesis, transfer, and microcavity assembly. (a) Growth of a WS_2 monolayer by CVD. (b) Transfer of the WS_2 monolayer onto the DBR. (c) Microcavity structure with integrated liquid crystal.

The microcavity consisted of two distributed Bragg reflectors (DBRs), forming a Fabry–Pérot cavity. For the DBR design, we used two kinds of materials with a large refractive index contrast: SiO_2 ($n = 1.46$) and Ta_2O_5 ($n = 2.14$). The thickness of each layer was determined by the formula $d = \lambda/4n$, where λ is the central wavelength, n is the refractive index of the material, and d is the layer thickness. With a central wavelength set to 620 nm, the calculated thicknesses were approximately 106.2 nm for SiO_2 and 72.4 nm for Ta_2O_5. To achieve high reflectivity at a specific wavelength, these layers were alternately stacked in a periodic manner. Starting with a soda-lime glass substrate coated with a conductive ITO layer, a 72.4 nm thick Ta_2O_5 layer was deposited using electron-beam evaporation, followed by a 106.2 nm thick SiO_2 layer. This combination formed one period. Each DBR consisted of 10 such periods of Ta_2O_5/SiO_2 multilayers, achieving reflectivity over 99% within the photonic stop band. The total length of the microcavity was approximately 1 μm, determined by both the polymer spacer and the liquid crystal layer.

To enable tunability, we introduced nematic liquid crystal E7 as a refractive index modulation medium inside the cavity. E7 exhibited a birefringence of about 0.2 ($\Delta n \approx 0.2$) at room temperature, and its molecular orientation could be reoriented under an external electric field, thereby altering the optical properties. Specifically, a polymethyl methacrylate (PMMA) alignment layer of approximately 230 nm thickness was spin-coated onto the transferred DBR surface. The same process was applied to the other DBR. Both DBRs were then rubbed with the same force to align the liquid crystal molecules in a uniform direction. After alignment, the two DBRs were assembled and bonded using UV-curable adhesive. To ensure

the cavity thickness matched the design from simulations, a uniform and controlled pressure was applied, which was monitored with a pressure sensor. At this stage, a thin air gap remained between the DBRs. Liquid crystal was introduced via capillary action using a capillary filling method, completing the WS_2 liquid crystal microcavity fabrication. Conductive clips were attached to the ITO-coated sides of the upper and lower DBRs to apply voltage across the cavity. The power supply used to apply voltage was a square-wave voltage source, capable of adjusting the voltage in increments of 0.1 V using a knob. This changed the orientation of the liquid crystal molecules, thereby modulating the coupling between optical modes.

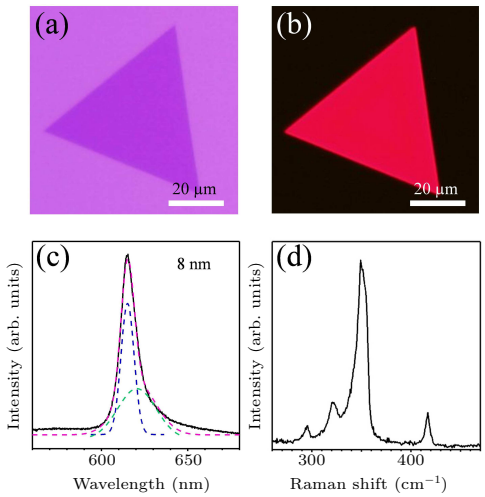


Fig. 2. Raman and PL characterization of monolayer WS_2. (a) Optical image of a monolayer WS_2. Scale bar: 20 μm. (b) PL image of a monolayer WS_2. Scale bar: 20 μm. (c) PL spectra collected from the region shown in Fig. 2(a). The multi-peak fit displays two distinct peaks: the neutral exciton (blue dashed line) and the trion (green dashed line). (d) Raman spectra collected from the same region as Fig. 2(a). The Raman spectra measured for the monolayer WS_2 (black curve) show unambiguous characteristic peaks at 350 and 417 cm^{-1}, which are consistent with previously reported results for WS_2.

Before transferring the monolayer, we characterized the photoluminescence (PL) properties of WS_2. Optical and PL images were obtained under a white-light microscope and a fluorescence microscope, as shown in Figs. 2(a) and 2(b). The CVD-grown WS_2 monolayers were triangular with smooth and intact surfaces and an average side length of about 60 μm, making them suitable for optical measurements.[22] The PL images revealed strong and uniform emission, indicating high optical quality. The PL spectrum was measured using a commercial confocal PL setup, showing a clear emission peak at 614 nm with a full width at half maximum (FWHM) of 8 nm. Multi-peak fitting revealed a neutral exciton peak and a trion peak, a typical feature of monolayer TMDs,[23] as shown in Fig. 2(c). Figure 2(d) shows the Raman spectrum obtained at room temperature, with peaks at 350 cm^{-1} and 417 cm^{-1}. The peak separation of 67 cm^{-1} confirmed that the sample was monolayer WS_2.[24]

3. Results and discussion

To achieve electrical control over exciton polaritons, we apply different voltages across the two ends of the fabricated microcavity. Figures 3(a)–3(c) show the exciton polariton dispersion relations of the WS_2-integrated liquid crystal microcavity under different voltages. An electric field is applied perpendicularly to the sample plane via the cavity, which tunes the refractive index of the liquid crystal layer and thereby shifts the energy of the cavity modes. In this experiment, we excite the sample at room temperature using a 410 nm laser with a power of 120 μW. We collect angle-resolved photoluminescence signals using a commercial optical setup to obtain the polariton dispersion curves. To further analyze the coupling behavior, we fit the experimental dispersion with the coupled oscillator model. This model treats the exciton and cavity photon as two coupled harmonic oscillators and introduces a coupling strength to solve for the system's eigenstates.[25] The polariton dispersion is modeled using the following equation:

$$\begin{pmatrix} E_{\mathrm{Cn}}(\theta) & \Omega \\ \Omega & E_{\mathrm{S}} \end{pmatrix} \begin{pmatrix} A \\ B \end{pmatrix} = E \begin{pmatrix} A \\ B \end{pmatrix}. \tag{1}$$

Here, Ω is the coupling strength, $E_{\mathrm{Cn}}(\theta)$ is the cavity mode energy, and E_{S} is the exciton energy.[26] The Hopfield coefficients ($|A|^2$ and $|B|^2$) describe the photon and exciton fractions of the polariton state. By diagonalizing the Hamiltonian, we obtain the new eigenenergies of the system, corresponding to the upper and lower polariton branches:

$$E_{\mathrm{UP}} = \frac{1}{2}\left(E_{\mathrm{S}} + E_{\mathrm{Cn}}(\theta)\right) + \frac{1}{2}\sqrt{\left(E_{\mathrm{S}} - E_{\mathrm{Cn}}(\theta)\right)^2 + 4\Omega^2}, \tag{2}$$

$$E_{\mathrm{LP}} = \frac{1}{2}\left(E_{\mathrm{S}} + E_{\mathrm{Cn}}(\theta)\right) - \frac{1}{2}\sqrt{\left(E_{\mathrm{S}} - E_{\mathrm{Cn}}(\theta)\right)^2 + 4\Omega^2}. \tag{3}$$

We fit the dispersion curves using these equations and the results match the experimental data very well, as shown in Figs. 3(a)–3(c). Under applied voltages of 1 V, 7 V and 10 V, we observe a clear evolution in the dispersion behavior.[27] At low voltage (Fig. 3(a), 1 V), the cavity mode energy closely matches the exciton energy, forming distinct upper (UP1) and lower (LP1, LP2) polariton branches. When the angle becomes larger, the lower polariton branch flattens, indicating the existence of a strong coupling regime. As we increase the voltage (Fig. 3(b), 7 V and Fig. 3(c), 10 V), the birefringence of the liquid crystal reduces the effective refractive index, leading to a blue shift of the cavity polariton mode energy. This decreases the detuning ($\Delta = E_{\mathrm{cav}} - E_{\mathrm{S}} < 0$) between the cavity and exciton modes, and the dispersion shifts accordingly. The LP1 branch also shows a blue shift, demonstrating that the applied electric field effectively tunes the light–matter coupling state.

We also measure the horizontal and vertical polarization components (I_1 and I_2) of the dispersion under different voltages and calculate the linear polarization degree

$P = (I_1 - I_2)/(I_1 + I_2)$, as shown in Figs. 3(d)–3(f). The red and black curves represent the horizontal and vertical components, respectively. As the voltage increases from 1 V to 10 V, the horizontally polarized dispersion (red curves) shifts continuously toward higher energy, while the vertically polarized branch (black curves) remains fixed, which results in an increased energy splitting between LP1 and LP2. This behavior is consistent with the cavity mode trend reported in Refs. [28,29]. This phenomenon results from the reorientation of the liquid crystal under the electric field, which selectively regulates the horizontally polarized polariton modes.[30,31] Furthermore, we analyze the exciton and photon fractions in the LP1 branch under different voltages, as shown in Figs. 3(g)–3(i). Using the Hopfield coefficients extracted from the dispersion fitting, we find that with increasing voltage, the energy detuning decreases, leading to an increased exciton fraction and a decreased photon fraction in the LP1 branch.[32] This trend further confirms that the applied voltage modulates the polariton composition and dispersion by tuning the position of the cavity mode.[33]

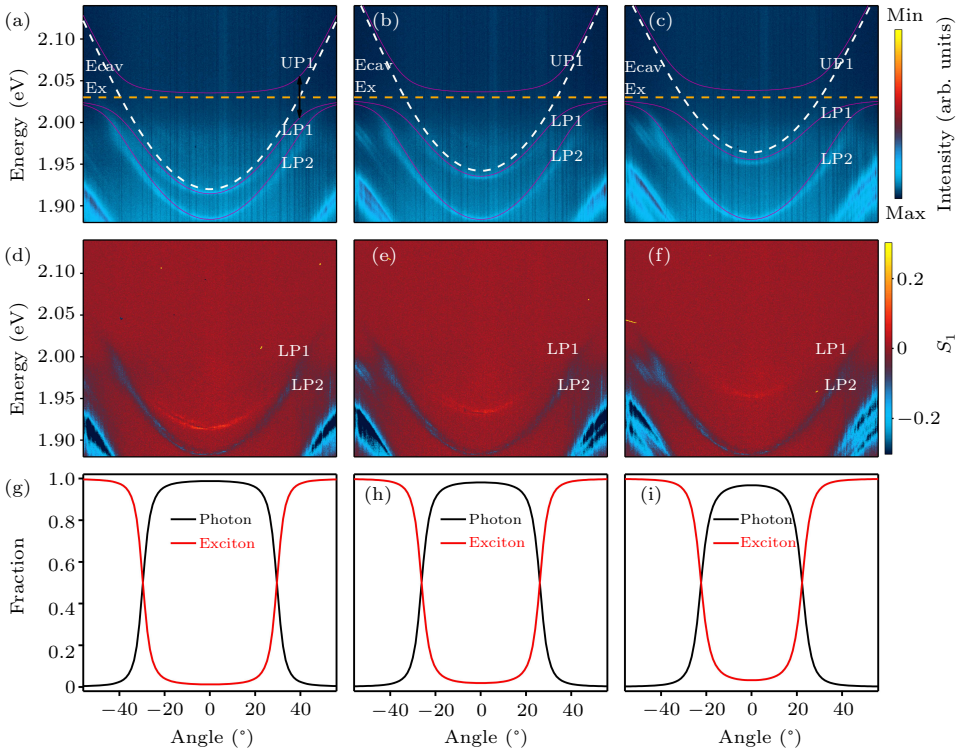


Fig. 3. Exciton polariton behavior in a liquid crystal microcavity. (a)–(c) Angle-resolved dispersion relations at 1 V, 7 V, and 10 V. Purple lines indicate fitted upper/lower polariton branches, orange dashed lines indicate exciton energy, and white dashed lines show cavity mode energy. Based on the fitted dispersion, we estimate a Rabi splitting of 50 meV for the exciton polariton branch (LP1), with detuning values of −110 meV (LP1 at 1 V), −88 meV (LP1 at 7 V), and −66 meV (LP1 at 10 V). The exciton resonance energy is determined to be 2.03 eV. (d)–(f) Degree of linear polarization, calculated from horizontal and vertical components. (g)–(i) Photon–exciton composition of the LP1 branch at different voltages.

To verify the anisotropy of the polarization response, we rotate the microcavity 90° clockwise and re-measure the angle-resolved dispersion and linear polarization degree under different voltages (1 V, 7 V, and 10 V), as shown in Figs. 4(a)–4(f). Figures 4(a)–4(c) show the dispersion curves and corresponding coupled oscillator model fits after rotation, while Figs. 4(d)–4(f) show the calculated linear polarization distributions under the same conditions. The fitted results reveal that the system still maintains strong coupling even after rotating the cavity by 90°, indicating that the coupling behavior is directionally robust. However, compared to the unrotated case, the polarization distribution changes significantly. The spatial pattern of linear polarization rotates by approximately 90°, with the dominant component shifting from the horizontal to the vertical orientation. This observation confirms that the refractive index tuning of the liquid crystal under an electric field is directionally dependent and closely related to the orientation of the cavity structure.

Figures 5(a)–5(b) present the energy variation of the LP1 under different applied voltages. The red curve corresponds to the measurements taken before rotating the microcavity, while the blue curve represents the results after a 90° clockwise rotation. It can be observed that, as the voltage increases from 1 V to 10 V, the LP1 energy exhibits a continuous upward trend regardless of the rotation, indicating that the applied voltage effectively tunes the energy position of the polaritons. This energy tuning is mainly attributed to the shift of the cavity mode induced by the electrically controlled liquid crystal,

which alters the effective refractive index of the cavity and consequently adjusts the photon energy, leading to the movement of the polariton branches. Overall, the rotation operation does not disrupt the strong coupling regime, confirming the repeatability and directional tunability of the liquid crystal microcavity system.[34]

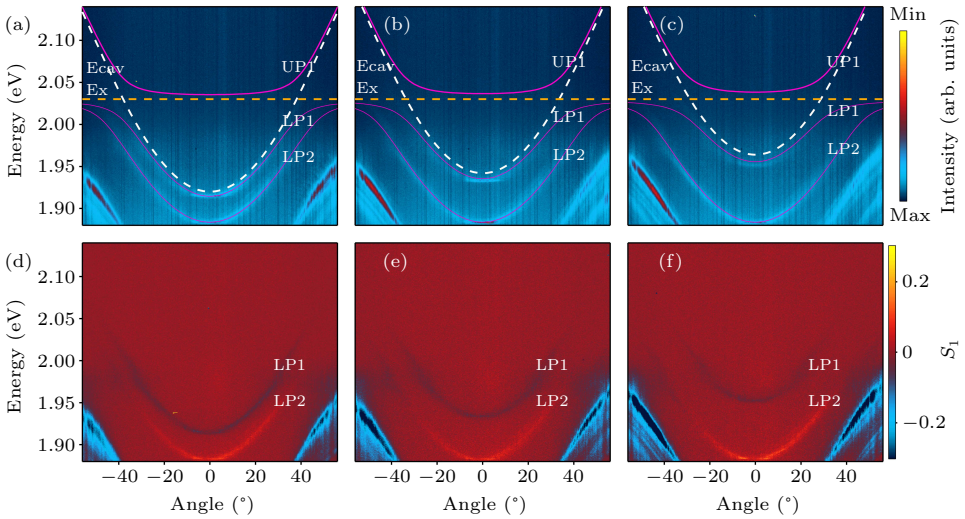


Fig. 4. Exciton polariton behavior in a liquid crystal microcavity after 90° clockwise rotation. (a)–(c) Angle-resolved dispersion at 1 V, 7 V, and 10 V with fitted polariton branches (purple lines), exciton energy (orange dashed line), and cavity mode energy (white dashed line). (d)–(f) Linear polarization degree, calculated from horizontal and vertical components corresponding to (a)–(c), indicating directionally dependent polarization rotation.

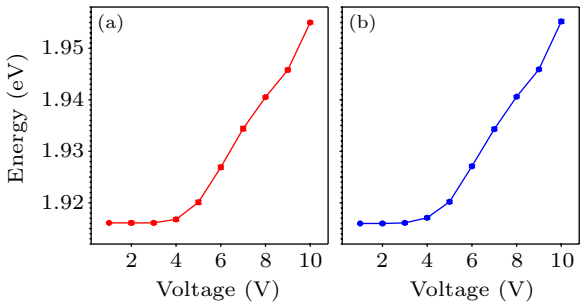


Fig. 5. Energy evolution of the LP1 under applied voltages from 1 V to 10 V. (a) Energy of LP1 before rotation. (b) Energy of LP1 after a 90° rotation.

4. Conclusion

We have successfully synthesized monolayer WS_2 using the CVD method and confirmed its high quality through Raman and PL spectroscopy. By employing transfer techniques combined with liquid crystal integration, we constructed an electrically tunable optical microcavity. We investigated the exciton–polariton dispersion under applied voltages of 1 V, 7 V, and 10 V. Through dispersion fitting, linear polarization analysis, and component decomposition, we confirmed the presence of strong light–matter coupling and demonstrated efficient electrical tuning within the strong coupling regime in the LC-integrated microcavity. Our work provides both a practical approach and experimental insight into the electrical control of exciton polaritons in optical microcavities at room temperature. Moreover, this study lays a solid foundation for the realization of tunable polaritonic lasers and valleytronic devices operable under ambient conditions.

Acknowledgments

This work was supported by the National Natural Science Foundation of China (Grant Nos. 12174285 and 12474315). H. Dai also acknowledges support from the National Natural Science Foundation of China (Grant No. 62375200). X. Zhai acknowledges support from the National Natural Science Foundation of China (Grant No. 12504372) and the China Postdoctoral Science Foundation–Tianjin Joint Support Program (Grant No. 2025T003TJ). Z. Li acknowledges support from the National Natural Science Foundation of China (Grant No. 12404424).

References

[1] Xu X, Yao W, Xiao D and Heinz T F 2014 *Nat. Phys.* **10** 343
[2] Wang Q H, Kalantar-Zadeh K, Kis A, Coleman J N and Strano M S 2012 *Nat. Nanotechnol.* **7** 699
[3] Wang G, Chernikov A, Glazov M M, Heinz T F, Marie X, Amand T and Urbaszek B 2018 *Rev. Mod. Phys.* **90** 021001
[4] Splendiani A, Sun L, Zhang Y, Li T, Kim J, Chim C Y, Galli G and Wang F 2010 *Nano Lett.* **10** 1271
[5] Mak K F, Lee C, Hone J, Shan J and Heinz T F 2010 *Phys. Rev. Lett.* **105** 136805
[6] Ye Z, Cao T, O'Brien K, Zhu H, Yin X, Wang Y, Louie S G and Zhang X 2014 *Nature* **513** 214
[7] Xia F, Wang H and Jia Y 2014 *Nat. Commun.* **5** 4458
[8] Berkelbach T C, Hybertsen M S and Reichman D R 2013 *Phys. Rev. B* **88** 045318
[9] Lagerwall J P and Scalia G 2012 *Curr. Appl. Phys.* **12** 1387
[10] Shang J, Zhang X, Zhang V L, Zhang X and Yu T 2023 *ACS Photonics* **10** 2064
[11] Coker K, Zheng C, Arhin J R, Agyekum K O B O and Zhang W 2024 *Chin. Phys. B* **33** 037102
[12] Liu X, Galfsky T, Sun Z, Xia F, Lin E C, Lee Y H, Kéna-Cohen S and Menon V M 2015 *Nat. Photonics* **9** 30

[13] Amani M, Lien D H, Kiriya D, Xiao J, Azcatl A, Noh J, Madhvapathy S R, Addou R, Kc S, Dubey M, Cho K, Wallace R M, Lee S C, He J H, Ager J W, Zhang X, Yablonovitch E and Javey A 2015 *Science* **350** 1065

[14] Zhao J, Su R, Fieramosca A, Zhao W, Du W, Liu X, Diederichs C, Sanvitto D, Liew T C H and Xiong Q 2021 *Nano Lett.* **21** 3331

[15] Hao K, Moody G, Wu F, Dass C K, Xu L, Chen C H, Sun L, Li M Y, Li L J, MacDonald A H, Li X and Li J 2016 *Nat. Phys.* **12** 677

[16] Amani M, Taheri P, Addou R, Ahn G H, Kiriya D, Lien D H, Ager J W, Wallace R M and Javey A 2016 *Nano Lett.* **16** 2786

[17] Wang Y, Zhai X, Feng L and Gao T 2022 *Appl. Phys. Express* **15** 022005

[18] Zhan T, Shi X, Dai Y, Liu X and Zi J 2013 *Adv. Mater.* **24** 2320

[19] Lee Y H, Zhang X Q, Zhang W, Chang M T, Lin C T, Chang K D, Yu Y C, Wang J T W, Chang C S, Li L J and Lin T W 2012 *Adv. Mater.* **24** 2320

[20] Ling X, Lee Y H, Lin Y, Fang W, Yu L, Dresselhaus M S and Kong J 2014 *Nano Lett.* **14** 464

[21] Lan F, Yang R, Sun K, Wang Z, Zhang Y, Wang Y and Cheng H 2022 *Vacuum* **201** 111091

[22] Najmaei S, Liu Z, Zhou W, Zou X, Shi G, Lei S, Yakobson B I, Idrobo J C, Ajayan P M and Lou J 2013 *Nat. Mater.* **12** 754

[23] Mak K F, He K, Shan J and Heinz T F 2012 *Nat. Nanotechnol.* **7** 494

[24] Berkdemir A, Gutiérrez H R, Botello-Méndez A R, Perea-López N, Elías A L, Chia C I, Wang B, Crespi V H, López-Urías F and Charlier J C 2013 *Sci. Rep.* **3** 1755

[25] Savona V, Hradil Z, Quattropani A and Schwendimann P 1994 *Phys. Rev. B* **49** 8774

[26] Malpuech G, Kavokin A, Di Carlo A, Baumberg J J, Compagnone F, Lugli P and Zamfirescu M 2002 *Phys. Status Solidi A* **190** 181

[27] Chakraborty C, Kinnischtzke L, Goodfellow K M, Beams R and Vamivakas A N 2015 *Nat. Nanotechnol.* **10** 507

[28] Fernandez H A, Withers F, Russo S and Barnes W L 2019 *Appl. Phys. Lett.* **115** 071101

[29] Rechcińska K, Król M, Mazur R, Morawiak P, Mirek R, Łempicka K, Bardyszewski W, Matuszewski M, Kula P, Piecek W, Szczytko J and Pacuski W 2019 *Science* **366** 727

[30] Choi S W, Yamamoto S I, Iwata T and Kikuchi H 2009 *J. Phys. D: Appl. Phys.* **42** 112002

[31] Zhai X, Ma X, Gao Y, Xing C, Gao M, Dai H, Wang X, Pan A, Schumacher S and Gao T 2023 *Phys. Rev. Lett.* **131** 136901

[32] Flatten L C, He Z, Coles D M, Trichet A A P, Powell A W, Taylor R A, Warner J H and Smith J M 2016 *Sci. Rep.* **6** 33134

[33] Gogna R, Zhang L, Wang Z and Deng H 2019 *Opt. Express* **27** 22700

[34] Sun Z, Gu J, Ghazaryan A, Shotan Z, Considine C R, Dollar M, Chakraborty B, Liu X, Ghaemi P and Kéna-Cohen S 2017 *Nat. Photonics* **11** 491